The Astrophysical Journal, 994:103 (14pp), 2025 November 20 https://doi.org/10.3847/1538-4357/adfbe5

Signatures of Confined and Eruptive Solar Flares in Microwave Spectra

E. W. Cliver[1], M. Kazachenko[1,2,3], H. S. Hudson[4,5], T. Alberti[6], M. Laurenza[7], S. M. White[8], and P. T. Gallagher[9]
[1] National Solar Observatory, 3665 Discovery Drive, Boulder, CO 80303, USA
[2] Laboratory for Atmospheric and Space Physics, University of Colorado Boulder, 3665 Discovery Drive, Boulder, CO 80303, USA
[3] Department of Astrophysical and Planetary Sciences, University of Colorado Boulder, 2000 Colorado Ave, CO 80305, USA
[4] SUPA School of Physics and Astronomy, University of Glasgow, Glasgow G12 8QQ, UK
[5] Space Sciences Laboratory, University of California, Berkeley, CA 94720, USA
[6] Istituto Nazionale di Geofisica e Vulcanologia, via di Vigna Murata 605, 00143 Roma, Italy
[7] Institute of Space Astrophysics and Planetology—INAF, Via del Fosso del Cavaliere 100, 00133 Roma, Italy
[8] Space Vehicles Directorate, Air Force Research Laboratory, Kirtland AFB, Albuquerque, NM 87117, USA
[9] Astronomy & Astrophysics Section, Dublin Institute for Advanced Studies, DIAS Dunsink Observatory, Dublin, D15 XR2R, Ireland
Received 2025 April 3; revised 2025 August 5; accepted 2025 August 9; published 2025 November 18

Abstract

We describe how microwave spectra of confined flares differ from those of eruptive flares. All 29 confined ⩾M1.4 soft X-ray flares from NOAA Active Region 12192 in 2014 October that were observed by the Radio Solar Telescope Network in the >300 MHz microwave range (encompassing RSTN frequencies from 410 to 15,400 MHz) had low-frequency (⩾410 MHz) cutoffs in their peak-flux-density spectra, with peak emission <10 solar flux units (sfu) at 410 MHz. Wind/Waves observations at 1 MHz for 20 of these cutoff microwave bursts suggest that few, if any, of the 29 flares were accompanied by escaping electrons. We find a marked difference between microwave spectra for samples of intense (⩾M5) confined and eruptive flares from 2011 to 2016: 20 of 21 confined ⩾M5 flares had cutoff spectra, while 27 of 30 ⩾M5 eruptive flares had peak 410 MHz emission >10 sfu (with a median value of 431 sfu). For the subsets of these events with Wind/Waves observations, only one of 20 confined events was unambiguously accompanied by 1 MHz emission, while 25 of the 29 eruptive flares had peak 1 MHz fluxes $>10_3$ sfu (above a background of ∼200–400 sfu), with an overall median peak value of $\sim 10_5$ sfu. These results indicate that strong confined flares characteristically do not involve or affect open field lines, ruling out interchange reconnection as a confined-flare generation mechanism, leaving reconnection between closed loops as the likely alternative. The microwave spectral signatures of confined and eruptive flares have potential application for the determination of confinement/eruption for flares on solar-type stars.

Unified Astronomy Thesaurus concepts: Solar radio flares (1342); Solar coronal mass ejections (310)

1. Introduction

Eruptive flares, i.e., those with associated coronal mass ejections (CMEs), are the main drivers of space weather at Earth (S. W. Kahler 1992; J. T. Gosling 1993; M. Temmer 2021; E. W. Cliver et al. 2022a). Beyond direct coronagraph observations, there are a variety of remote and in situ noncoronagraphic indicators of eruptive flares (H. S. Hudson & E. W. Cliver 2001). Remotely sensed indicators include long-duration soft X-ray (SXR) bursts (N. R. Sheeley et al. 1975; S. Kahler 1977), slow-drift metric type II bursts and EUV waves (E. W. Cliver et al. 1999, 2004; A. M. Veronig et al. 2010), postflare, or more accurately, posteruption loop systems (R. A. Kopp & G. W. Pneuman 1976; Z. Švestka 2007; K. Shibata & T. Magara 2011), and coronal dimmings (D. M. Rust 1983; H. S. Hudson et al. 1995; A. M. Veronig et al. 2025). In situ manifestations of CMEs include gradual solar energetic proton (SEP) events (S. W. Kahler et al. 1978; M. Desai & J. Giacalone 2016), sudden-commencement (SC) type geomagnetic storms (J. T. Gosling et al. 1991), and Forbush decreases of cosmic ray intensity (H. V. Cane 2000). Each of the principal remotely sensed indicators have shortcomings: there is no well-defined SXR flare duration that distinguishes between eruptive and noneruptive flares (N. R. Sheeley et al. 1983; R. A. Harrison 1995); slow (⩽400 km s^{-1}) CMEs characteristically lack type II associations (J. T. Gosling et al. 1976; N. Gopalswamy 2006); not all fast CMEs produce type II bursts (N. Gopalswamy et al. 2008); and postflare loops and coronal dimmings are not routinely, or systematically, reported by the ground- and space-based solar flare patrols. The energetic CMEs required for near-Earth in situ effects are dependent on such factors as flare location for SEP events (K. G. McCracken 1962; E. W. Cliver et al. 2020) and SC-type storms (H. W. Newton 1943; S.-I. Akasofu & S. Yoshida 1967) and magnetic field orientation in the CME for storms (J. W. Dungey 1961; D. H. Fairfield & L. J. Cahill 1966).

Solar flares are generally divided into two classes: eruptive flares (with associated CMEs; Z. Švestka & E. W. Cliver 1992) and confined flares without CMEs (R. Pallavicini et al. 1977; R. L. Moore et al. 2001). Comparative counts of flares and CMEs indicate that confined flares are more plentiful because of the relative absence of CMEs for the more common lower-energy flares (S. Yashiro et al. 2006), e.g., Hα subflares and C-class and smaller SXR events. Interest in confined flares increased with the disk passage of NOAA Active Region 12192 in 2014 October. From October 18–29, this region produced 35 ⩾M-class flares, of which 31 (including six X-class events) were confined (H. Chen et al. 2015; X. Sun et al. 2015; J. K. Thalmann et al. 2015; T. Li et al. 2020,

2021).[10] Although, in retrospect, there are hints of similarly strong flare confinement in large groups during cycle 18 (1944–1954; E. W. Cliver et al. 2022b), NOAA AR 12192 provides the best-documented evidence of such behavior. This led to searches for various diagnostics of eruption versus confinement in large flares and the active regions from which they arise. These include such parameters as: active region magnetic flux (T. Li et al. 2020, 2021); the flux swept by flare ribbons (J. K. Thalmann et al. 2015); the proximity of the flaring region to the center of active regions (Y. Wang & J. Zhang 2007; X. Cheng et al. 2011; H. Chen et al. 2015; J. Tschernitz et al. 2018); average ribbon separation distances and ribbon peak separation speeds (H. Kurokawa 1989; A. M. Veronig & W. Polanec 2015; M. D. Kazachenko et al. 2022a, 2022b; M. D. Kazachenko 2023); and flare temperature and energy partition (H. R. M. Kay et al. 2003; Z. M. Cai et al. 2021; S. W. Kahler & A. G. Ling 2022; M. D. Kazachenko 2023). E. A. Avallone & X. Sun (2020) find that, for confined flares, the polarity inversion line tends to have lower magnetic shear and weaker net ribbon currents. As reviewed by M. D. Kazachenko et al. (2022a), two magnetic parameters are currently thought to determine whether a solar flare will be eruptive or confined: active region free (nonpotential) energy and the constraining effect of the overlying field.

Here we examine flare microwave spectra in the decimetric–centimetric range from 300 to ∼15,000 MHz as a discriminator between comparably intense confined and eruptive events. Previous studies have examined the microwave and lower frequency spectra of smaller samples of confined flares: N. Gopalswamy et al. (2009; 13 X-class CME-less flares from 2000 to 2005); K. L. Klein et al. (2010; 15 X-class CME-less flares from 2000 to 2005); C.-M. Tan et al. (2021; 10 M-class confined flares from 12192). For data samples, we considered in turn: (a) 29 ⩾M1.4 (new scaling; H. Hudson et al. 2024b) confined flares (including eight X-class events) and four M-class eruptive flares (with jet and/or CME) from NOAA AR 12192; and (b) samples of 21 ⩾M5 (including 10 X-class) confined flares (13 from 12192) and 29 ⩾M5 (14 X-class) eruptive flares, both from the M. D. Kazachenko et al. (2023) 2010–2016 database. Since the launch of the Large Angle and Spectrometric Coronagraph (LASCO) coronagraph on the Solar and Heliospheric Observatory (SOHO) in late 1995, the utility of noncoronagraphic indicators of CMEs has largely been rendered moot for space weather forecasting purposes. The current constellation of satellite-borne coronagraphs (SOHO LASCO; G. E. Brueckner et al. 1995 and STEREO SECCHI; M. L. Kaiser et al. 2008) is capable of detecting ∼100% of CMEs (A. Vourlidas et al. 2020). This is not the case, however, for superflares on solar-type stars where CMEs can only be detected indirectly by noncoronagraphic methods (S.-P. Moschou et al. 2019; A. M. Veronig et al. 2021, 2025; K. Namekata et al. 2022).

Our analysis is presented in Section 2, and the findings are interpreted in Section 3. Results are summarized and discussed in Section 4.

[10] The GOES soft X-ray (SXR) classification scheme is defined as follows: GOES classes A1–9 through X1-9 correspond to flare peak 1–8 Å fluxes of $(1-9)\times 10^{n}$ W m^{-2} where $n=[-8,-7,-6,-5,-4]$, for classes A, B, C, M, and X, respectively. Flares with peak fluxes $\geqslant 10^{-3}$ W m^{-2} are referred to as ⩾X10 events, e.g., X25. All of the SXR classes in this study correspond to the new scaling in which the peak fluxes of events occurring prior to 2017 have been multiplied by a factor of 1.43 (J. Machol et al. 2022; H. Hudson et al. 2024b).

2. Analysis

2.1. Data

Our data source for the microwave spectra was the US Air Force's Radio Solar Telescope Network (RSTN; D. A. Guidice et al. 1981), which monitors the Sun at eight frequencies: 245, 410, 606, 1415, 2695, 4995, 8800, and 15,400 MHz. The four RSTN stations are located at Sagamore Hill (MA, USA), Palehua (HI, USA), Learmonth (Australia), and San Vito (Italy). The 1 s digitized data are available at https://www.ngdc.noaa.gov/stp/space-weather/solar-data/solar-features/solar-radio/rstn-1-second/. For lower frequencies, we used 940 KHz observations (referred to here as 1 MHz) from Wind/Waves (J.-L. Bougeret et al. 1995) available at https://cdaweb.gsfc.nasa.gov/pub/data/wind/waves/ that can be converted to solar flux units (sfu; 1 sfu = 10^{-22} W m^{-2} Hz^{-1}) as in M. Laurenza et al. (2009). We used the RSTN data set for microwave bursts because of the worldwide (24 hr) coverage of the Air Force patrol in conjunction with Wind/Waves ∼1 MHz observations from L1. Other data sets (e.g., Nobeyama (H. Nakajima et al. 1985; M. Shimojo & K. Iwai 2023) and Hiraiso (T. Kondo et al. 1995) microwave data and STEREO S/Waves (J. L. Bougeret et al. 2008) ∼1 MHz data) can also be used to produce radio time profiles and spectra such as those in Figure 1.

2.2. Confined and Eruptive ⩾M1.4 Flares from NOAA AR 12192

Table 1 (adapted from H. Chen et al. 2015) gives the SXR and radio parameters for 35 ⩾M1.4 SXR flares, including eight X-class events, from NOAA AR 12192. Our SXR intensities differ from those in Chen et al. because we applied the recent 1.43 upward adjustment by NOAA to GOES 1–8 Å intensities from 1975–2016 (H. Hudson et al. 2024b). Of the 35 events in the Chen et al. list, adequate RSTN data for spectrum evaluation were available for 33 events. Of these 33 events, H. Chen et al. (2015) classified 29 as confined and four as eruptive because of their association with EUV jets observed on 304 Å filtergrams obtained by the Atmospheric Imaging Assembly (J. R. Lemen et al. 2012) on SDO. One of these four events was also associated with a CME.

All of the 29 confined events from NOAA AR 12192 had a microwave peak flux-density spectrum that was cut off at low frequencies, i.e., for each of these 29 events, weak (<10 sfu) or no emission was observed below their spectral peak (8800 MHz or 15,400 MHz for 27 cases) beginning at a "cutoff" frequency that ranged from 4995 to 410 MHz. In contrast, three of the four eruptive events had emission that extended down to 410 MHz; while the fourth (No. 26 in Table 1) was cut off at 606 MHz but had emission at 410 MHz. For the 29 cutoff events from NOAA AR 12192, the most common cutoff frequencies were 606 MHz and 1415 MHz. For each of the 29 confined flares, peak 410 MHz emission was <10 sfu after background subtraction of the 1 s flux level at the time of the onset of the flare SXR emission. For 21 of these 29 events, this emission was ⩽1 sfu (column (12) in Table 1). Time-intensity traces for the eight RSTN frequencies for the eight X-class flares in Table 1 (all confined) are given in the top panels of Figure 1, and the Wind/Waves 1 MHz traces are given in the middle panels. The general background flux at 1 MHz of ~ 2–4×10^{2} sfu was subtracted to obtain the peak values > 100 sfu given in column (15) of Table 1. The

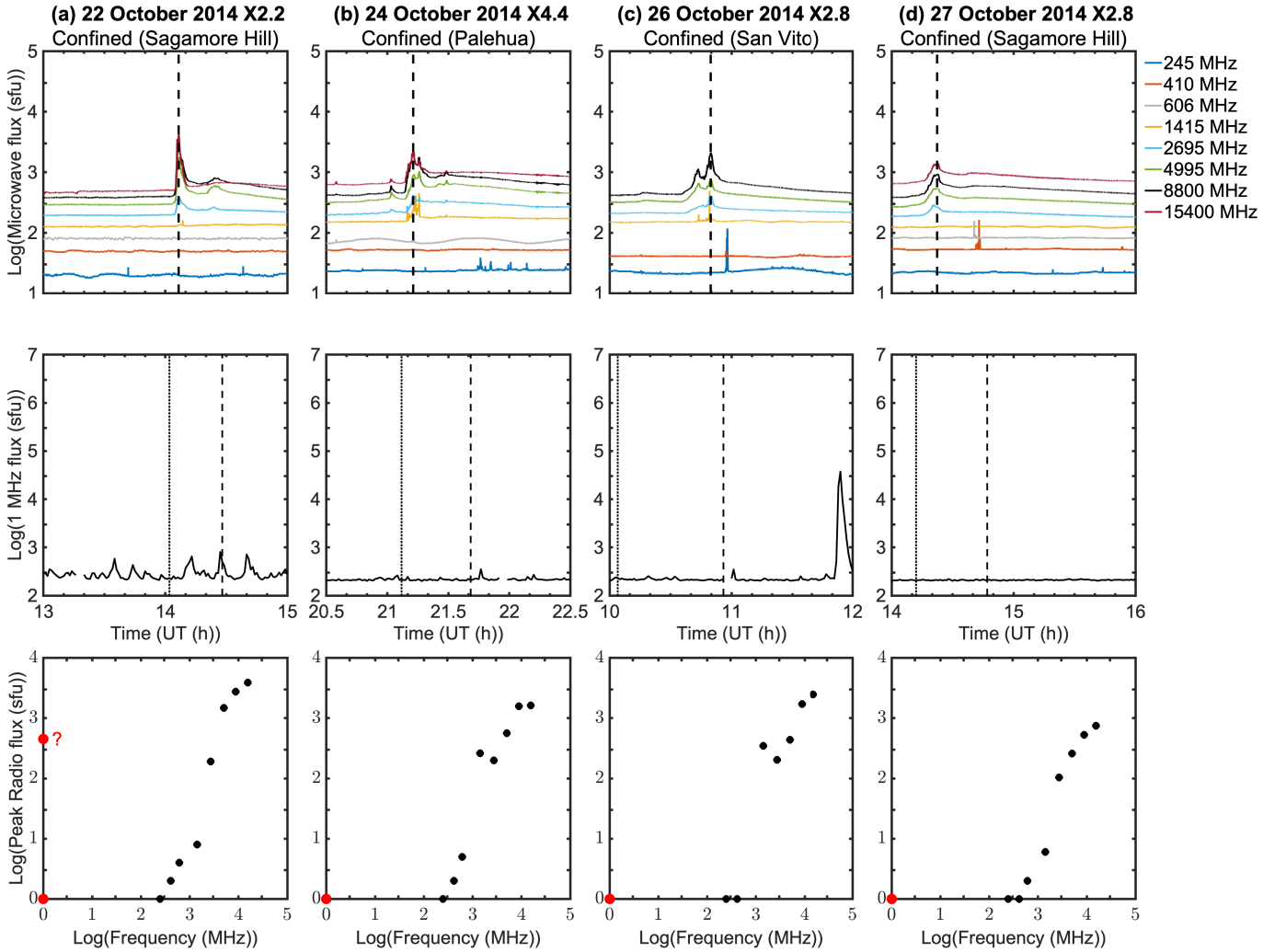

Figure 1. (Top panel for each event) Time profiles of flux density at the eight RSTN frequencies for the eight confined X-class flares from NOAA AR 12192. In each case, the low-frequency emission at the time of peak high-frequency microwave flux is cut off at a frequency ⩾410 MHz. (Middle) Time trace of Wind/Waves 1 MHz emission. (Bottom) 1–15,400 MHz peak flux radio spectra for each event, with the 1 MHz peak flux plotted in red on the y axis (see text for explanation of the two 1 MHz values in (a), (e), and (h)). The dashed lines indicate the time of peak 4995–15,400 MHz emission (top panel) and the onset and peak of 1–8 Å SXR emission (middle).

1–15,400 MHz spectrum of each event is given in the bottom panel. Zero and negative flux values after background (based on the onset of flare SXR emission) subtraction are plotted at $y = 1$. Dashed vertical lines indicate the time of peak emission in the 4995–15,400 MHz range (top panel) and the onset and peak of the associated 1–8 Å SXR events (middle panel).[11] While RSTN provides an essential operational radio patrol of the Sun, the intercalibrations among the four stations are rather loose and the records for all stations occasionally have missing frequencies (e.g., Figure 1(c)) or other artifacts such as oscillatory traces (Figures 1(b), (h)) or spurious spikes, as documented in the notes to Tables 1–3.

The microwave peak flux spectrum is based on the timing of the principal peak in the high-frequency range (4995-15,400 MHz) of RSTN patrol frequencies (column (9) in Table 1). The peak values for the other RSTN frequencies are taken to be the largest (background-corrected) value within ±2 minutes of this time. This is a compromise between an instantaneous spectrum and a true peak-flux-density spectrum that yields representative "cutoff" and "non-cutoff" spectra for samples of confined and eruptive flares. In our classification of microwave spectra, we did not consider the 245 MHz trace in the metric range. The frequent low-level noise-storm-type activity at 245 MHz was generally not a factor at 410 MHz. As we will show, a 410 MHz peak flux of <10 sfu is a good indicator of flare confinement.

The Wind/Waves 1 MHz traces in Figure 1 (and for the other 16 confined events from NOAA AR 12192 observed by Wind) indicate that the emission in confined flares rarely extends to 1 MHz (the nominal plasma frequency at a height of ∼7 $R_\odot$; Y. Leblanc et al. 1998). For event No. 11 in Table 1 (Figure 1(a)) , that had the strongest 1 MHz emission (∼4.0 × 10^2 sfu at 14:13 UT) that could be associated with any microwave burst in Figure 1, there are other comparable peaks (at ∼13:35 and 14:40 UT) within the 2 hr time window that are not clearly related to the higher-frequency emission in the top panel. For this reason, there are two 1 MHz points in the

[11] Uncompressed figures of the microwave and 1 MHz time profiles for each event in Tables 1–3 are given in T. Alberti & E. W. Cliver (2025).

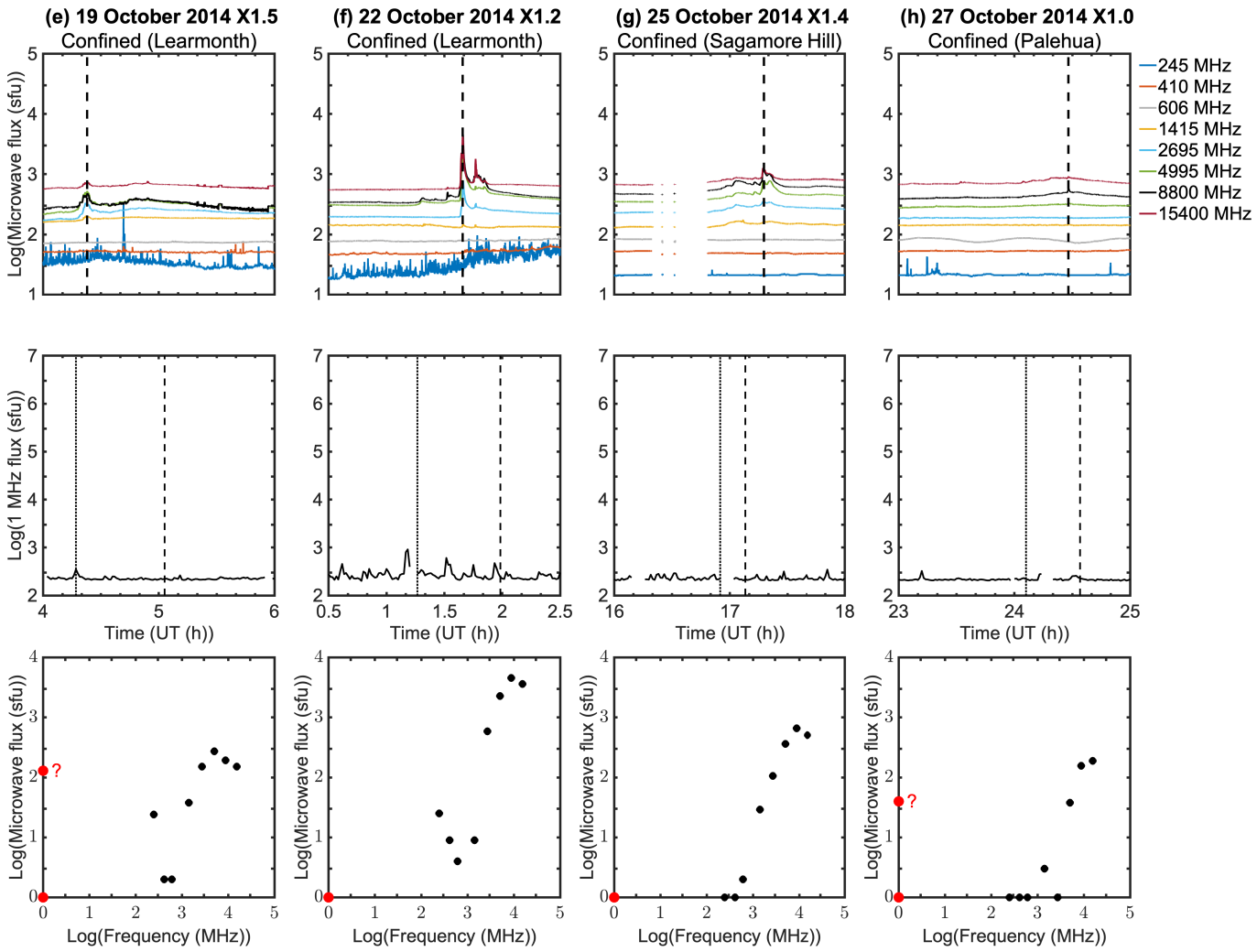

Figure 1. (Continued.)

bottom panel of Figure 1(a), one at 0 sfu and a non-zero value flagged with a "?". Two 1 MHz points are also used to illustrate the "signal or noise?" uncertainty for smaller 1 MHz increases (∼100 and ∼40 sfu) for two other confined flares (Nos. 2; Figure 1(e)) and 21; Figure 1(h)), respectively, with each of the non-zero peak flux values in these two events flagged with a question mark. Based on examination of the microwave and 1 MHz time profiles in Figure 1 and T. Alberti & E. W. Cliver (2025), there is no compelling/unambiguous evidence that any of the 20 confined flares in Table 1 with cutoff spectra and Waves coverage are associated with 1 MHz emission.

Figures 2(a)–(d) contain microwave and 1 MHz intensity-time profiles and 1–15,400 MHz spectra for the four eruptive events identified by H. Chen et al. (2015) in Table 1. Jets were observed for all of these events at 304 Å, and a CME was recorded for the event in Figure 2(c). For events (a)–(c), the low-frequency emission at the time of peak high-frequency emission extends to 410 MHz. For event (d), emission is cut off at 606 MHz, but reappears at 410 MHz. The peak 245 MHz emission exceeds 10^4 sfu for the events in Figures 2(a) and (b) (top panel). Contrary to expectations, the Waves 1 MHz emission during the associated SXR and microwave bursts for these two events is weak or absent, while moderate to strong 1 MHz emission is observed in close time agreement with these emissions for the events in Figures 2(c) and (d). H. Chen et al. (2015) located the two events in Figures 2(a) and 2(b) in a subregion (labeled L1) that was spatially separated from that (L2) for the events in Figures 2(c) and (d), with both L1 and L2 on the periphery of 12192.

2.3. Confined and Eruptive ⩾M5 Flares in NOAA Active Regions from 2011–2016

In this subsection, we consider lists of intense (⩾M5) confined and eruptive flares extracted from the 2010–2016 "ribbon database" of M. D. Kazachenko et al. (2017)[12], described in M. D. Kazachenko (2023). Because the analysis in M. D. Kazachenko et al. (2017) was based on optical magnetograph observations, the ribbon database compilation consists of flares that occurred within 45° of the solar central meridian.

Table 2 lists the SXR, Hα, and radio parameters for the 21 confined ⩾M5 flares (10 X-class); from M. D. Kazachenko et al. (2017), with sufficient RSTN data to determine their microwave spectrum. These 21 events originated in seven separate spot groups, with 13 events from NOAA AR 12192

[12] http://solarmuri.ssl.berkeley.edu/~kazachenko/RibbonDB/

Table 1
⩾M1.4 Flares from NOAA AR 12192 in 2014 October

No.	Date 2014	Start Time (UT)[a]	Peak Time (UT)[a]	Duration (minutes)[a]	GOES SXR Class[b]	Jet/CME?	RSTN Station	MICROWAVE Spectral Peak			410 MHz Peak Flux (sfu)[c]	Low-Freq. Cutoff Spectrum?	Cutoff Frequency (MHz)	Peak 1 MHz		Comments
								(UT)	(GHz)	(sfu)[c]				Flux (sfu[d])	Time (UT)[d]	
1	Oct 18	7:02	07:58	107	M2.2	No	Learmonth	07:49:00	5	150	−4	Yes	606	—	—	
2	Oct 19	4:17	05:03	91	X1.5	No	Learmonth	04:22:47	5	273	3	Yes	606	~100	04:17	(a)
3	Oct 20	9:00	09:11	20	M5.5	No	Learmonth	09:05:58	15	1504	5	Yes	1415	—	—	(b)
4	Oct 20	16:00	16:37	55	M6.4	No	Sagamore Hill	16:09:08	9	657	2	Yes	606	~100	16:07	
5	Oct 20	18:55	19:02	9	M2.0	Jet (L1)	Sagamore Hill	18:58:56	9	171	236	No	…	—	—	(c)
6	Oct 20	19:53	20:04	20	M2.4	No	Sagamore Hill	19:57:20	9	522	2	Yes	1415	~100	20:11	
7	Oct 20	22:43	22:55	30	M1.7	No	Learmonth	22:46:32	15	168	1	Yes	1415	—	—	
8	Oct 21	13:35	13:38	5	M1.7	Jet (L1)	Sagamore Hill	13:37:20	9	1202	241	No	…	—	—	(c)
9	Oct 22	1:16	01:59	72	X1.2	No	Learmonth	01:39:27	9	4589	9	Yes	606	~300	1:32	(d)
10	Oct 22	5:11	05:17	10	M3.8	No	Learmonth	05:14:34	15	1941	2	Yes	2695	N/A	N/A	
11	Oct 22	14:02	14:28	48	X2.2	No	Sagamore Hill	14:06:31	15	3900	2	Yes	606	~400	14:13	
12	Oct 23	9:44	09:50	12	M1.5	No	Learmonth	09:47:49	9	360	1	Yes	2695	~100	09:48	(a)
13	Oct 24	7:37	07:48	16	M5.7	Jet(L2) CME	Learmonth	07:42:11	9	1369	68	No	…	~2.0E+05	7:45	(a,e)
14	Oct 24	21:07	21:41	66	X4.4	No	Palehua	21:12:43	15	1637	2	Yes	410	—	—	(f)
15	Oct 25	16:55	17:08	76	X1.4	No	Sagamore Hill	17:17:39	9	659	0	Yes	606	~100?	17:28? gap	
16	Oct 26	10:04	10:56	74	X2.8	No	San Vito	10:49:44	15	2489	0	Yes	410 or 606	~100?	11:01? gap	(g)
17	Oct 26	17:08	17:17	22	M1.4	No	Sagamore Hill	17:09:44	9	631	0	Yes	606	—	—	
18	Oct 26	18:07	18:15	13	M6.0	No	Sagamore Hill	18:08:36	15	962	0	Yes	4995	—	—	
19	Oct 26	18:43	18:49	13	M2.7	No	Sagamore Hill	18:46:46	15	101	0	Yes	2695	—	—	
20	Oct 26	19:59	20:21	46	M3.4	No	Palehua	20:06:13	9	237	1	Yes	1415	—	—	(f)
21	Oct 27	0:06	00:34	38	X1.0	No	Palehua	00:27:58	15	189	0	Yes	2695	—	—	(f)
22	Oct 27	1:44	02:02	27	M1.4	No	Palehua	02:02:27	15	52	1	Yes	2695	—	—	(f)
23	Oct 27	3:35	03:41	13	M1.8	No	Learmonth	N/A	N/A	N/A	N/A	N/A	N/A	—	—	(h)
24	Oct 27	9:59	10:09	27	M9.5	No	Learmonth	10:02:47	15	121	1	Yes	1415	—	—	
25	Oct 27	14:12	14:47	57	X2.8	No	Sagamore Hill	14:22:22	15	745	1	Yes	606	—	—	
26	Oct 27	17:33	17:40	14	M2.0	Jet (L2)	Sagamore Hill	17:37:00	9	133	20	Yes	606	~3.7E+03	17:40	(i)
27	Oct 28	2:15	02:42	53	M4.8	No	Palehua	02:36:47	15	92	-2	Yes	410	N/A	N/A	
28	Oct 28	3:23	03:32	18	M9.4	No	Palehua	03:33:32	15	236	-1	Yes	606	N/A	N/A	
29	Oct 28	13:54	14:06	29	M2.2	No	Sagamore Hill	13:59:40	15	98	1	Yes	1415	N/A	N/A	
30	Oct 29	6:03	08:20	169	M1.4	No	Learmonth	08:16:41	15	48	0	Yes	1415	N/A	N/A	(b)
31	Oct 29	9:54	10:01	12	M1.7	No	San Vito	09:57:37	9	64	1	N/A	N/A	N/A	N/A	(j)
32	Oct 29	14:24	14:33	27	M2.0	No	Sagamore Hill	14:30:32	15	149	0	Yes	1415	N/A	N/A	(k)
33	Oct 29	16:06	16:20	27	M1.4	No	Sagamore Hill	16:09:45	15	94	1	Yes	2695	N/A	N/A	
34	Oct 29	18:47	18:50	5	M1.8	No	Sagamore Hill	18:49:36	15	77	0	Yes	2695	N/A	N/A	
35	Oct 29	21:18	21:22	7	M3.2	No	Palehua	21:21:38	15	73	0	Yes	4995	N/A	N/A	

Notes. Comments: (a) 4995 and 8800 MHz traces closely track each other; (b) 1415 and 2695 MHz time profiles are essentially identical; (c) H. Chen et al. (2015) jet event; L1 location in 12192; (d) microwave peak near onset of weak low-frequency event; (e) H. Chen et al. (2015) jet/CME event; L2 location in 12192; (f) weak oscillations around 606 MHZ baseline level; (g) no 606 MHz observations; (h) data gap at all frequencies from 03:30:11 to 03:38:48 UT; (i) H. Chen et al. (2015) jet event; L2 location in 12192; (j) 410/606 MHz data corrupted/missing; (k) intense (up to ∼10,000 sfu) 410 emission in the Sagamore Hill trace not observed at San Vito.

[a] Timing data from: https://www.ngdc.noaa.gov/stp/space-weather/solar-data/solar-features/solar-flares/x-rays/goes/xrs/ (NOAA definitions in Veronig et al. 2022).

[b] New GOES scaling (H. Hudson et al. 2024b).

[c] Above intensity at the onset of the SXR emission.

[d] — indicates weak (<100 sfu) 1 MHz emission above background near the time of the microwave burst.

Table 2
⩾M5 Confined Flares from 2010 to 2016 (Kazachenko et al. 2023)

No.	Date[a] (mm/dd/yy)	GOES SXR Class[b] (W m^{-2})	GOES Start Time (UT)[c]	GOES Peak Time (UT)[c]	GOES Duration (minutes)[c]	Hα Lon (deg)	Hα Lat (deg)	NOAA Active Region	RSTN Station	Spectral Peak			410 MHz Peak Flux (sfu)[d]	Low-freq. Cutoff spectrum?	Cutoff Frequency (MHz)	Peak 1 MHz		Comments
										(UT)	(GHz)	(sfu)[d]				Flux (sfu[e])	Time (UT)[e]	
1	03-09-11	2.06E-04	23:13	23:23	16	9	8	11166	Learmonth	23:22:53	9	663	8	Yes	606	~200	23:34	
2	09-08-11	9.25E-05	15:32	15:46	20	40	14	11283	San Vito	15:43:12	15	432	84	No	...	8.0E +04	15:43	(a)
3	07-05-12	5.32E-05	03:25	03:36	14	23	−17	11515	Palehua	03:35:21	9	122	2	Yes	1415	~100	3:32	(b)
4	01-07-14	1.00E-04	10:07	10:13	30	−11	−13	11944	San Vito	10:11:59	9	5994	0	Yes	410 or 606	~100	10:18	(c)
5	02-02-14	6.08E-05	09:24	09:31	12	−13	−11	11967	Learmonth	09:28:09	15	356	2	Yes	410	8.8E +03	9:31	
6	02-04-14	5.29E-05	01:16	01:23	15	14	−13	11967	Learmonth	01:20:33	9	43	4	Yes	1415	—	—	(b)
7	02-04-14	6.99E-05	03:57	04:00	9	6	−14	11967	Learmonth	03:58:49	9	198	2	Yes	2695	—	—	(b)
8	10-19-14	1.50E-04	04:17	05:03	91	-58	-10	12192	Learmonth	04:22:47	5	273	3	Yes	606	~100	4:17	(d)
9	10-20-14	5.49E-05	09:00	09:11	20	−43	−13	12192	Learmonth	09:05:58	15	1504	5	Yes	1415	—	—	(e)
10	10-20-14	6.44E-05	16:00	16:37	55	−37	−14	12192	Sagamore Hill	16:09:08	9	657	2	Yes	606	~100	16:07	
11	10-22-14	1.25E-04	01:16	01:59	72	−19	−14	12192	Learmonth	01:39:27	9	4589	9	Yes	606	~300	1:32	(f)
12	10-22-14	2.37E-04	14:02	14:28	48	−13	−14	12192	Sagamore Hill	14:06:31	15	3900	2	Yes	606	~400	14:13	
13	10-24-14	4.54E-04	21:07	21:41	66	21	−16	12192	Palehua	21:12:43	15	1637	2	Yes	410	—	—	(g)
14	10-25-14	1.47E-04	16:55	17:08	76	31	−16	12192	Sagamore Hill	17:17:39	9	659	0	Yes	606	~100?	17:28? gap	
15	10-26-14	2.85E-04	10:04	10:56	74	40	−18	12192	San Vito	10:49:45	15	2489	0	Yes	410 or 606	~100?	11:01? gap	(h)
16	10-26-14	5.88E-05	18:07	18:15	13	34	−16	12192	Sagamore Hill	18:08:36	15	962	0	Yes	4995	—	—	
17	10-27-14	1.00E-04	00:06	00:34	38	44	−14	12192	Palehua	00:27:58	15	189	0	Yes	2695	—	—	(g)
18	10-27-14	9.5E-05	09:59	10:09	27	48	−18	12192	Learmonth	10:02:47	15	121	1	Yes	1415	—	—	
19	10-27-14	2.8E-04	14:12	14:47	57	52	−17	12192	Sagamore Hill	14:22:22	15	745	1	Yes	606	—	—	
20	10-28-14	9.4E-05	03:23	03:32	18	61	−14	12192	Palehua	03:33:32	15	236	−1	Yes	606	N/A	N/A	
21	12-04-14	8.72E-05	18:05	18:25	51	32	−20	12222	Sagamore Hill	18:25:54	9	68	14	Yes	1415	~450	18:23	(i)

Notes. Comments: (a) possible jet; (b) no 15,400 MHz observations; (c) spurious high (~10^4 sfu) 606 values; (d) 4995 and 8800 MHz traces closely track each other; (e) 1415 and 2695 MHz time profiles are essentially identical; (f) microwave peak near onset of weak low-frequency event; (g) weak oscillations around 606 MHZ baseline level; (h) no observations at 606 MHz; (i) 606 MHZ observations missing after 17:46:06 UT

[a] Two flares on 2009 May 9 and 10, classified as confined in the Kazachenko et al. database, occurred during a gap in LASCO coverage.

[b] M. D. Kazachenko (2023); new GOES scaling (H. Hudson et al. (2024b)

[c] From: https://www.ngdc.noaa.gov/stp/space-weather/solar-data/solar-features/solar-flares/x-rays/goes/xrs/ (NOAA definitions in A. Veronig et al. 2002).

[d] Measured from the intensity at the time of the SXR onsetXR onset:

[e] — indicates weak (<100 sfu) emission above background near the time of of the microwave burst.

Table 3
⩾M5 Eruptive Flares from 2011 to 2016 (Kazachenko et al. 2023)[a]

No.	Date	GOES Peak Class[b]	GOES Start Time[c] (UT)	GOES Peak Time[c] (UT)	GOES Dur.[c] (minutes)	Lon (deg)	Lat (deg)	NOAA Active Region	RSTN Station	Spectral Peak			410 MHz Peak Flux (sfu)[d]	Cutoff Spectrum?	1 MHz peak		CME		Comments
										(UT)	(GHz)	(sfu)[d]			(UT)	(sfu)	Speed (km s^{-1})	Width (deg)	
1	02-15-11	3.17E-04	01:44	01:56	22	10	−20	11158	Learmonth	1:55:46	9	1314	6115	No	02:00	5.0E+04	669	360	
2	08-03-11	8.66E-05	13:17	13:48	53	30	16	11261	San Vito	13:32:33	5	171	878	No	13:30	6.0E+05	610	360	
3	08-04-11	1.28E-04	03:41	03:57	23	36	19	11261	Learmonth	3:53:35	9	2480	2045	No	04:04	1.5E+06	1315	360	
4	09-25-11	5.01E-05	15:26	15:33	12	−43	16	11302	Sagamore Hill	15:31:12	9	121	985	No	15:34	2.0E+04	676	67	(a)
5	09-26-11	5.31E-05	05:06	05:08	7	−34	13	11302	Learmonth	5:06:28	9	578	7	Yes	05:19	2.5E+02	689	48	(b)
6	10-02-11	5.45E-05	00:37	00:50	22	12	9	11305	Learmonth	0:43:49	5	183	75	No	00:52	2.0E+05	259	103	
7	01-23-12	1.25E-04	03:38	03:59	56	21	28	11402	Learmonth	3:50:53	9	6945	297	No	03:48	1.5E+05	2175	360	
8	03-07-12	7.67E-04	00:02	00:24	38	−29	17	11429	Palehua	0:21:15	9	20362	364	No	00:28	2.5E+06	2684	360	(c)
9	03-07-12	1.96E-04	01:05	01:14	18	-20	17	11429	Palehua	1:14:31	9	13837	622203	No	01:27	2.8E+03	1825	360	(c)
10	03-10-12	1.21E-04	17:15	17:44	75	18	18	11429	Palehua	17:35:08	9	641	498	No	17:46	⩽1.0E+05	1296	360	(c)
11	07-02-12	7.70E-05	10:43	10:52	14	−8	−17	11515	San Vito	10:47:46	5	628	215	No	10:49	3.5E+02	313	125	(d,e)
12	07-12-12	2.03E-04	15:37	16:49	113	1	−15	11520	Sagamore Hill	16:53:25	5	477	2783	No	16:42	1.5E+05	843	76	
13	04-11-13	9.20E-05	06:55	07:16	34	−12	9	11719	Learmonth	7:10:00	5	305	232	No	07:04? gap	⩾2.0E+07?	861	360	
14	10-28-13	6.16E-05	15:07	15:15	14	−26	−8	11882	Sagamore Hill	15:10:48	9	422	576	No	15:14	1.5E+06	812	360	
15	02-12-14	5.35E-05	*03:55*	04:25	46	2	−12	11974	Learmonth	4:24:52	15	110	145	No	04:32	1.8E+03	373	360	(f)
16	03-29-14	1.34E-04	17:35	17:48	19	32	11	12017	Sagamore Hill	17:46:34	9	1186	1134	No	17:50	4.0E+06	528	360	(a)
17	04-18-14	1.04E-04	12:31	13:03	59	28	−19	12036	San Vito	12:54:39	5	1183	2109	No	12:57	2.0E+06	1203	360	(d)
18	08-25-14	5.57E-05	20:06	20:21	23	38	9	12146	Sagamore Hill	20:17:15	9	351	35	No	20:43?	8.0E+02?	711	177	
19	09-08-14	6.52E-05	23:12	00:29	139	−29	12	12158	Palehua	23:50:31	5	239	711	No	00:02	2.5E+05	920	360	(g)
20	09-10-14	2.36E-04	17:21	17:45	59	−2	14	12158	Sagamore Hill	17:33:06	5	2766	932	No	17:38	4.0E+06	1071, 1267	134, 360	
21	09-28-14	7.25E-05	02:39	02:58	40	23	−13	12173	Learmonth	2:46:57	5	261	47	No	02:58? gap	1.5E+02?	215	60	
22	11-07-14	2.23E-04	*17:00*	17:26	41	−33	15	12205	Palehua	17:21:40	9	395	335	No	17:30	⩾1.0E+05	795	293	(h)
23	12-18-14	9.64E-05	21:41	21:58	44	−8	−15	12241	Palehua	21:56:51	5	418	3765	No	21:58? gap	⩾6.0E+05?	1195	360	
24	12-20-14	2.63E-04	00:11	00:28	44	24	−21	12242	Palehua	0:22:00	9	3143	4	Yes	00:48? gap	3.0E+04?	830	257	(i,j)
25	03-11-15	3.02E-04	16:11	16:22	18	−21	−17	12297	Sagamore Hill	16:21:04	15	258	120	No	16:34?	1.3E+03?	240	74	(k)
26	06-22-15	9.41E-05	17:39	18:23	72	8	12	12371	Sagamore Hill	17:53:15	9	1602	1	Yes	18:13	1.5E+04	1209	360	(l,j)
27	06-25-15	1.07E-04	08:02	08:16	63	42	9	12371	Learmonth	8:14:29	9	10118	105	No	08:30	2.0E+04	1627	360	
28	11-04-15	5.30E-05	13:31	13:52	42	−3	6	12443	Sagamore Hill	13:41:20	5	531	21	No	13:58	4.5E+04	578	360	
29	11-09-15	5.57E-05	12:49	13:12	39	−41	−11	12449	Sagamore Hill	13:03:08	5	616	548	No	13:20	2.0E+05	1041	273	

Notes. Comments: (a) microwave burst time profile has impulsive jetlike time profile; (b) weak gradual rise-and-fall event at 410 MHz begins near peak of microwave burst; (c) no observations at 15,400 MHz; (d) high (∼1000–70,000 sfu) spurious values at 606 MHz all day at San Vito; (e) a spike in the 4995 MHZ trace (10:50:22–10:50:38 UT with peak flux of 10,395 sfu) was removed; (f) later 112 sfu 15,400 MHz peak at 04:33:02 UT; used minimum 15,400 MHz value of of 593 sfu at 03:55 UT peak because of San Vito data gap at 03:52 UT; (g) Kazachenko SXR event starts at 23:59 UT; (h) minimum 9 GHz time set to 17:18 UT (320 sfu); (i) low-frequency cutoff at 606 MHz; (j) a confined flare triggering a CME?; (k) microwave data gap from 16:12:53 to 16:18:26 UT, with 4 minutes 22 s offset; (l) low-frequency cutoff at 606 MHz.

[a] Five events were eliminated because of inadequate RSTN data (2011 February 13, 17:37 UT; 2011 September 6, 22:21 UT; 2011 September 7, 22:39 UT; 2012 March 9, 03:53 UT).

[b] New GOES scaling (H. Hudson et al. 2024b).

[c] From: https://www.ngdc.noaa.gov/stp/space-weather/solar-data/solar-features/solar-flares/x-rays/goes/xrs/ (NOAA definitions in A. Veronig et al. 2002); italics in start time column indicate that a slightly different time was used because of data availability;

[d] Measured above intensity at the time of the SXR onset (see (c)).

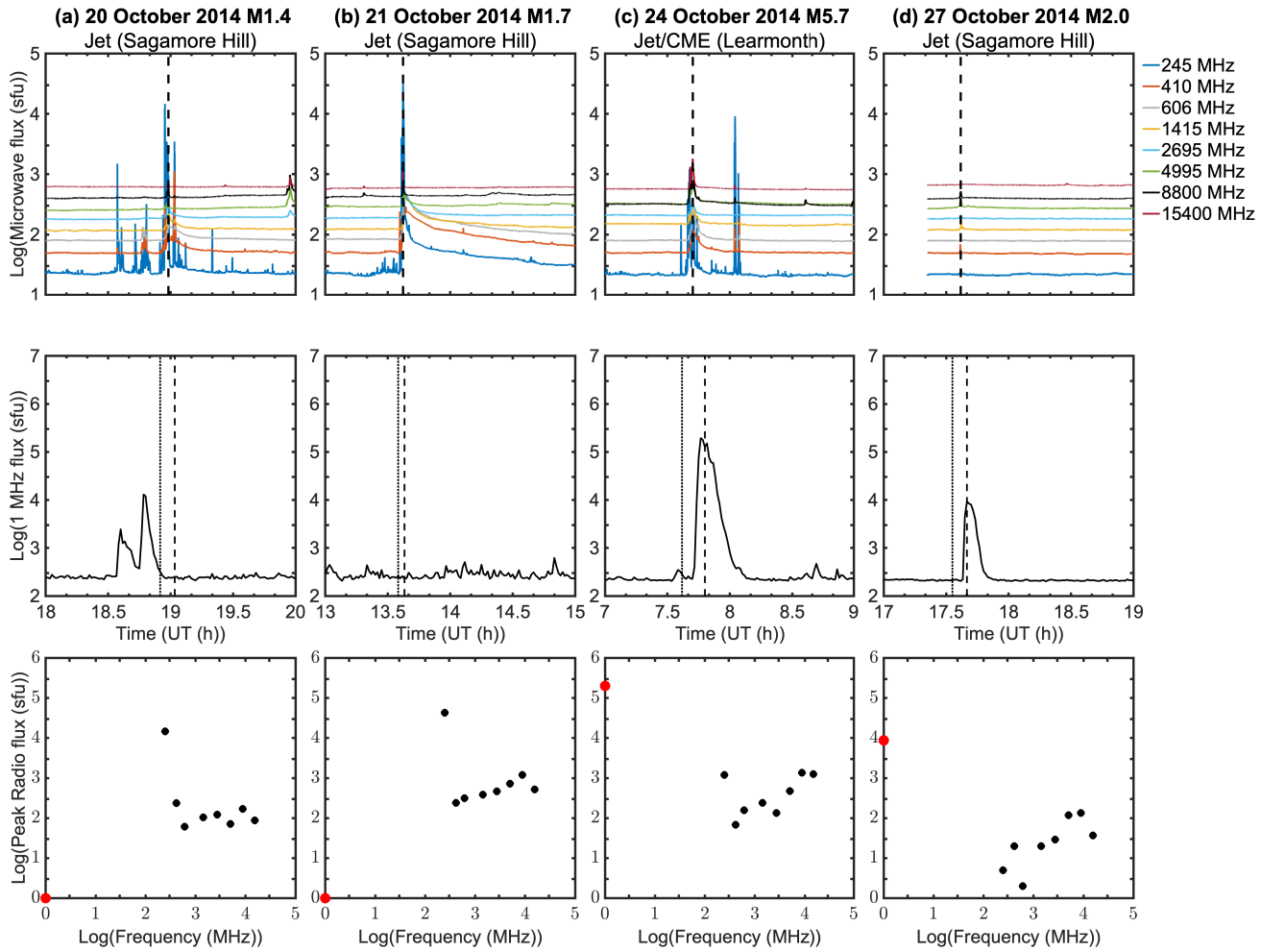

Figure 2. (Top panel for each event) Time profiles of flux density at the eight RSTN frequencies for the four eruptive flares from NOAA AR 12192. (Middle) Wind/Waves 1 MHz time traces. (Bottom) Composite radio spectrum for each event from 1 to 15,400 MHz. The dashed lines indicate the time of peak 4995–15,400 MHz emission (top panel) and the onset and peak of 1–8 Å SXR emission (middle).

(including four events that occurred at latitudes >45° from the central meridian). Of these 21 events, 20 had cutoff spectra, and 20 were observed by Wind/Waves. Of the 20 events with Wind/Waves coverage, the event shown in Figure 3 (No. 5 in Table 2 provides the strongest evidence that confined flares can have associated 1 MHz emission. We will return to this event below.

Table 3, also culled from the M. D. Kazachenko et al. (2017) ribbon database, lists the SXR, Hα, and radio parameters for 29 eruptive flares with SXR classes $\geqslant$M5. RSTN microwave time traces, along with Wind/Waves 1 MHz burst time profiles and 1–15,400 peak-flux-density spectra, are given in Figures 4(a)–(h) for eight representative eruptive events. For 26 of these 29 events, the microwave burst extended to 410 MHz, with a median peak intensity at that frequency of 431 sfu. The other three events had cutoff spectra. Of the 29 eruptive events, 25 had (back-ground subtracted) 1 MHz peak fluxes $>10_3$ sfu with a median peak flux of $\sim 10_5$ sfu (range from 150 to $\gtrsim 2 \times 10_7$ sfu).

The events in Tables 2 and 3 that defy expectations, viz., confined events with emission that extends to 410 MHz and eruptive events with cutoff spectra, are informative. Plots for three such counterexamples are given in Figures 5(a)–(c), with (a) (No. 2 in Table 2) for a confined flare and (b,c) (Nos. 24 and 26 in Table 3) for eruptives. The confined event in Figure 5(a) bears some resemblance to that in Figure 2(c) (No. 13 in Table 1), with its impulsive microwave and 1 MHz time profile. It is plausible that event No. 2 in Table 2, like event No. 13 in Table 1, had an associated jet-type CME. The LASCO CME catalog (N. Gopalswamy et al. 2024)[13] lists a relatively narrow (37°) CME in the northwest quadrant that was first observed at 16:36 UT at a height of $\sim 2.5\,R_\odot$. This event had an anomalously high peak 1 MHz emission ($\sim 10^5$ sfu) for a confined flare. Delayed enhancements of 410 MHz emission in both Nos. 24 and 26 in Table 3 suggest that a cutoff event triggered the eruption. Both of these events had a peak 1 MHz emission $\gtrsim 10^4$ sfu. For a fourth counter-example, eruptive event No. 5 in Table 3 with a cut-off spectrum, we note that the associated CME was located in the southwest solar quadrant with a position angle of 251° (width = 48°) while the associated flare was located in the northeast (N13E34). This was the only apparent misassociation we found for the events in Table 3.

The four counterexamples are conspicuous in a scatter plot in Figure 6 of peak high-frequency (4995–15,400 MHz) microwave flux density versus peak 410 MHz emission for

[13] https://cdaw.gsfc.nasa.gov/CME_list/.

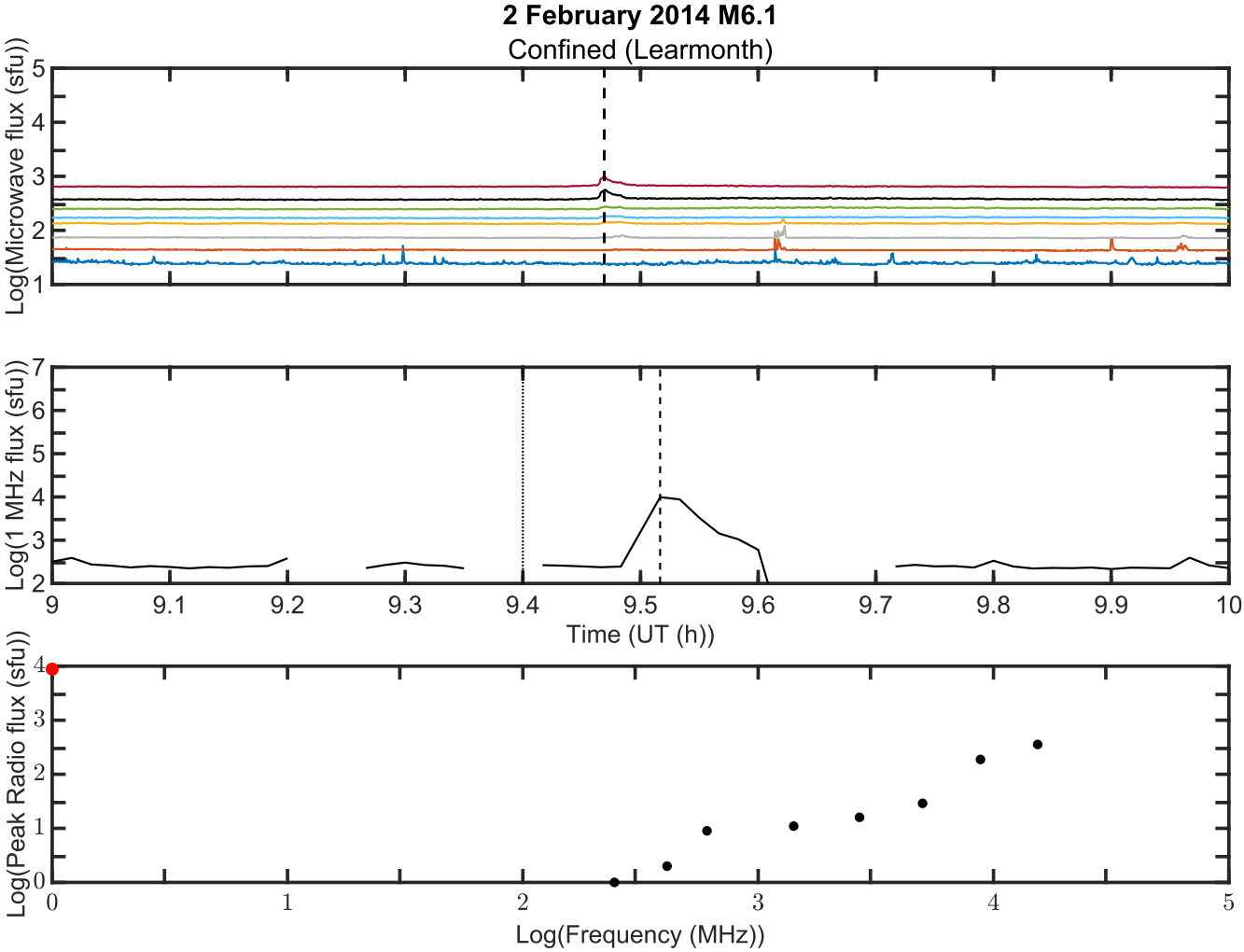

Figure 3. An unusual microwave burst (No. 5 in Table 2) with a cutoff spectrum and a significant (∼9000 sfu) 1 MHz burst.

the 21 ⩾M5 confined flares in Table 2 and the 30 ⩾M5 eruptive flares in Tables 1 and 3. Figure 7 is a histogram of the relative intensities of the 1 MHz emission for the 20 confined (Table 2) and 30 eruptive (with 1 event from Table 1 (No. 13; not included in the M.D. Kazachenko et al. (2017) data base and 29 events from Table 3) ⩾M5 flares we considered that had Wind/Waves coverage. The nominal median 1 MHz intensity in Figure 7 for the eruptive events (~10^5 sfu) is 1000 times that for the confined events (~10^2 sfu). The largest confined event in Figure 7 (No. 2 in Table 2; 1 MHz intensity = 8.0 x 10^4 sfu) was likely associated with a CME, leaving event No. 5 in Table 2 (8.8 x 10^3 sfu) as the strongest candidate for a confined flare with associated 1 MHz emission (Figure 3). That said, intense (~10^4 sfu) 1 MHz events can occur without a strong SXR flare or high-frequency microwave burst (Figures 1(c), 2(a), 4(a)), and the 1 MHz burst that is temporally associated with the confined event in Figure 3 may be the result of a chance alignment. The relative absence of 1 MHz emission in confined flares is not a result of the big flare syndrome (S. W. Kahler 1982) in which bigger flares (in this case, eruptive flares) have more associated phenomena. The strengths of the confined flares in Table 2 and eruptive flares in Table 3 are comparable. Ten of the 21 flares in Table 2 (vs. 14 of 30 in Table 3) were X-class SXR events, with a median intensity of M9.5 for both samples. The two groups were also similar in terms of microwave emission, with a median peak intensity of 659 sfu (597 sfu) for confined (eruptive flares).

In sum, there are marked differences in microwave spectra and 1 MHz emission between confined and eruptive flares, with a small number of exceptional cases. Confined events are characterized by low-frequency cutoffs between 410 MHz and 4995 MHz and weak, if any, 1 MHz emission, while eruptive flares have spectra that extend to 410 MHz and are typically accompanied by moderate to strong (10^4–10^7 sfu) 1 MHz emission. In general, the microwave burst morphologies for the cutoff and non-cutoff events are also different, with confined events having typically shorter durations and simpler time-intensity profiles vs. eruptive events which tend to be longer and more complex, with the spectral maxima of later peaks shifting to lower frequencies over time. In certain cases (e. g., 2012 January 23 (Figure 4(b)) and 2015 June 22 (Figure 5(c))), the strong later peaks likely reflect a change in emission mechanism from gyro-synchrotron emission to electron cyclotron maser emission (E. W. Cliver et al. 2011, 2022b; S. M. White et al. 2024). In general, as can be seen for the eruptive events in Figure 4, there is a rough correspondence between the microwave emission for large eruptive events (top panels of Figure 4) and the 1 MHz burst time profiles (middle panels), with the SXR start and peak times serving as crude fiducials for both frequency ranges.

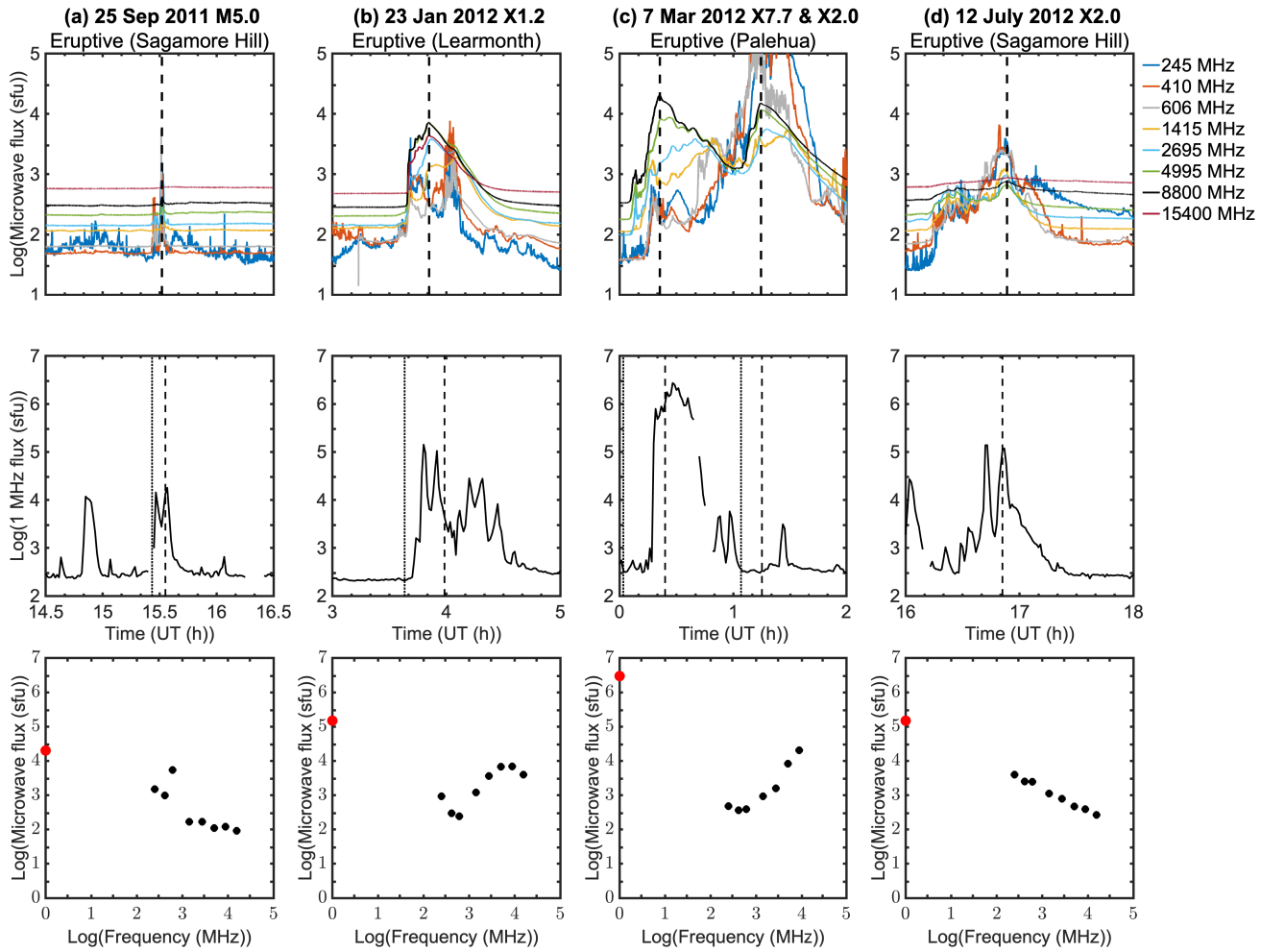

Figure 4. (Top panel for each event) Time profiles of flux density at the eight RSTN frequencies for eight ⩾M5 CME-associated flares from 2011 to 2016. (Middle) Associated 1 MHz intensity-time profiles. (Bottom) 1–15,400 MHz peak-flux-density spectra. In all cases, the low-frequency emission at the time of peak high-frequency emission flux extends downward to 410 MHz. The dashed lines indicate the time of peak 4995–15,400 emission (top panel) and the onset and peak of 1–8 Å SXR emission (middle).

3. Interpretation of Results

The virtual absence of 1 MHz emission for confined events indicates a lack of open fields in the flaring region. Such open fields would serve as conduits for flare-accelerated electrons that give rise to type III plasma emission at 1 MHz and lower frequencies. The absence of open fields rules out interchange reconnection (N. U. Crooker et al. 2002) as a flare generation mechanism for confined events because such reconnection occurs between open field lines and closed loops. The four flares from NOAA AR 12192 for which H. Chen et al. (2015) reported jets bear on this point because interchange reconnection is the preferred mechanism for the formation of such jets (M. Shimojo & K. Shibata 2000; S. W. Kahler et al. 2001).

It came as a surprise that, for two of the four flares with jets identified by H. Chen et al. (2015; Nos. 5 and 8 in Table 1; Figures 2(a) and (b)), radio emission did not extend to 1 MHz. The radio bursts associated with these two jets were particularly strong at 245 MHz (∼15,000 sfu (No. 5 in Table 1); ∼40,000 sfu (No. 8)), the lowest of the eight fixed RSTN frequencies. The fact that these two jets came from the same L1 location, while the other two jets, which had escaping electrons originating in L2, indicates that the cause of the absence of 1 MHz emission lay in the magnetic topology of the source subregion. We suggest that the "interchange reconnection" giving rise to the "radio-quiet" (at 1 MHz) bursts from L1 was between small and large closed loops rather than between small, closed loops and open field lines as in the standard picture for jets. The apparent confinement of ejected material to closed loops in these two events—evidenced by the lack of 1 MHz emission—identifies the jets as the high-energy counterpart of surges (R. C. Canfield et al. 1996) for which early Hα observations (Švestka 1976 (p.221)) showed that accelerated plasma travels outward, and returns, on the original trajectory, from sources at the edges of sunspot penumbrae.

4. Summary and Discussion

4.1. Summary

From an examination of microwave (∼400 MHz —∼15,000 MHz) spectra for: (1) ⩾M1.4 SXR class confined (CME-less) flares from NOAA AR 12192 in 2014 October, and (2) samples of confined and eruptive (CME-associated) ⩾M5 flares from multiple active regions for 2011–2016, we find that confined flares generally (29/29 cases for ⩾M1.4

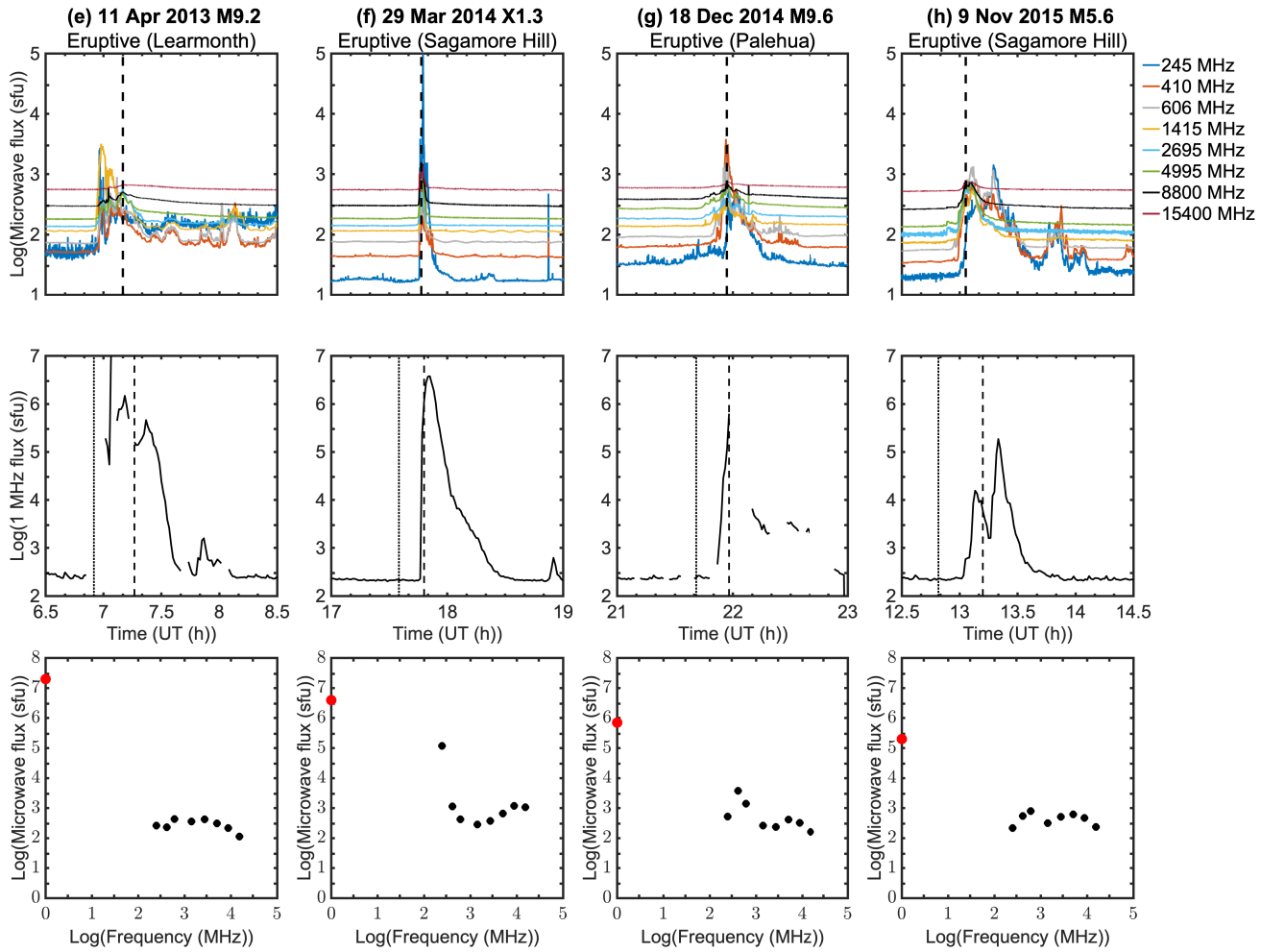

Figure 4. (Continued.)

flares from 12192 and 20/21 cases for ⩾M5 flares from 2011 to 2016) have microwave (>300 MHz) spectra that have a low-frequency cutoff between ∼400 and ∼5000 MHz while ⩾M5 eruptive flares characteristically (for 27 of 30 cases from 2011 to 2016) have microwave emission that extends to 410 MHz and lower frequencies. Strong (⩾M5) confined flares tend to have short, simple microwave time profiles dominated by a single peak, while eruptive flares have extended microwave bursts consisting of multiple peaks, with spectral maxima at progressively lower frequencies over time. Thus, microwave spectra and morphology can serve as an indicator of flare confinement/eruption in intense solar flares. To first order, intense eruptive flares give rise to strong 1 MHz emission (corresponding to radial distances from the Sun of $\sim 7\,R_\odot$) and confined flares do not. C.-M. Tan et al. (2021) previously reported the general absence of 1 MHz emission for a smaller sample of confined flares from 12192. We present evidence that some jets are surges that originate in reconnection between small- and large-scale loops.

4.2. Discussion

4.2.1. Loop–Loop Reconnection and Early Eruptive Flares

The lack of escaping electrons from confined flares implies an absence of open field lines connected to the flare site. This finding rules out interchange (closed-open) reconnection as the driving mechanism for magnetic energy release in confined flares, leaving reconnection between closed loops as the clearest alternative. The four eruptive events identified by H. Chen et al. (2015) are illuminating. All were located at the periphery of the active region. The two flares from subregion L1 (events (a) and (b) in Figure 2) lacked 1 MHz emission despite exceptionally strong emission ($\sim 10^4$ sfu) at 245 MHz. We attribute these two events to flare-induced surges, which typically originate at the edges of sunspot penumbrae (Švestka 1976). Surges are the ejection of cool material, observed in Hα to travel outward along curved field lines, returning by the same path. This behavior suggests closed–closed reconnection of a small loop with a large loop at the surge base. In contrast, the two flares from subregion L2 (events (c) and (d)) in Figure 3 were accompanied by moderate to strong 1 MHz emission, consistent with standard interchange reconnection.

The eruptive events we examined characteristically had strong 1 MHz emission that began between the onset and peak of the SXR flare, corresponding to the time of CME acceleration (J. Zhang et al. 2001). While the standard CSHKP reconnection of eruptive flares does not involve open field lines (see, e.g., Figure 1 of M. D. Kazachenko et al. 2022b), shock-accelerated electrons at the front and flanks of CMEs have immediate access to the heliosphere. Of the 29 eruptive flares in Table 3, 24 had CMEs with speeds >400 km s^{-1}, generally taken to be the threshold velocity for the generation of a coronal shock

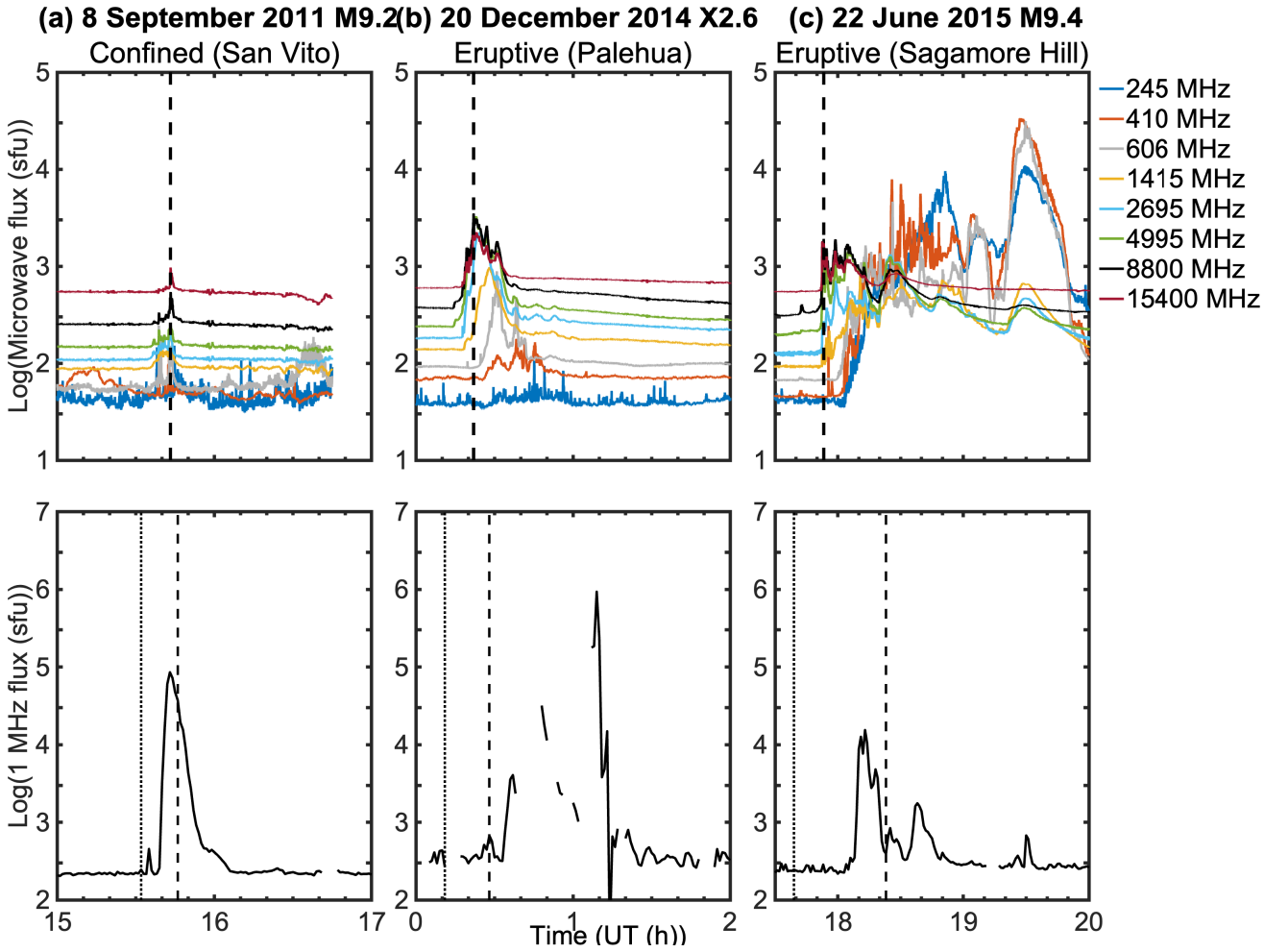

Figure 5. Time profiles of flux density at the eight RSTN frequencies (top panel) and Wind/Waves at 1 MHz (bottom) for three ⩾M5 SXR flare counterexamples from 2011–2016 to the dominant classification dichotomy found in this study, for which flares with low-frequency cutoffs in their peak-flux-density microwave spectrum were confined, and flares with emission that extended to 410 MHz were eruptive. Event (a) was plausibly associated with a jet-type CME (see text) while events (b) and (c) may be cases in which an initially confined flare triggered a CME. The dashed vertical lines indicate the time of peak 4995–15,400 emission (top panel) and the onset and peak of 1–8 Å SXR emission (bottom).

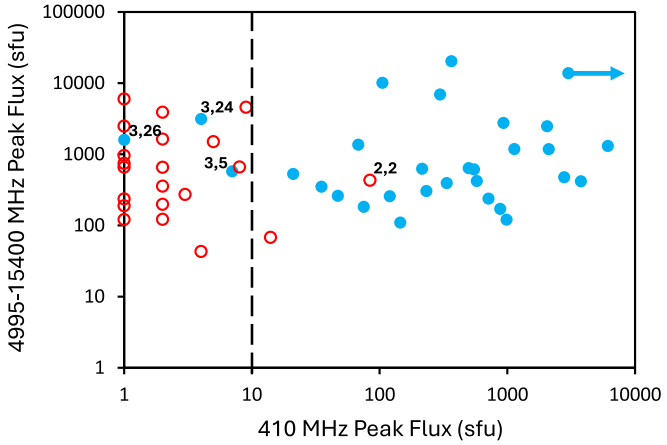

Figure 6. Scatter plot of the peak flux in the 4995–15,400 MHz range vs. the peak 410 MHz flux for samples of confined (Table 2; red data points) and eruptive ⩾M5 SXR flares (from Tables 1 and 3; blue). To first order, the dashed vertical line at 10 sfu separates the two populations. The labels refer to table and list numbers for four counter examples to the microwave spectral classification dichotomy of confined and eruptive solar flares.

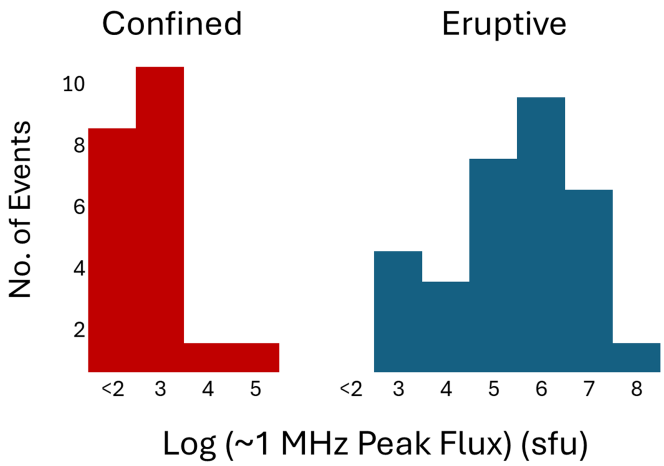

Figure 7. Histogram of the peak Wind/Waves 1 MHz emission for the confined and eruptive ⩾M5 flares in this study that were observed by Wind/Waves.

wave (J. T. Gosling et al. 1976; E. W. Cliver & E. D'Huys 2018). The median 1 MHz emission for these 24 events was $\sim 1.5 \times 10^5$ sfu versus $\sim 4 \times 10^2$ sfu for the five slower-speed events.

L. Sui et al. (2006) called attention to a class of "early impulsive flares" in which nonthermal >25 keV hard X-ray emission distinctly precedes the most rapid SXR increase (Sui et al. 2007). Such flares can depart from the observed close relationship found in the common Neupert effect (W. M. Neupert 1968; H. S. Hudson 1991; B. R. Dennis & D. M. Zarro 1993; H. S. Hudson et al. 2024a). Early impulsive flares, also termed "cold flares," are characterized by a very low thermal response relative to the nonthermal energy of accelerated particles. In a recent study of cold flares, A. L. Lysenko et al. (2023) determined the characteristics of ~100 such events, including 14 events from NOAA AR 12192. Cold flare characteristics that overlap with those of confined flares include high-frequency spectral maxima (15,400 MHz for 20 of 29 events in Table 1 and 11 of 21 events in Table 2 versus 2/29 for the Table 3 eruptive flares) and evidence for V. A. Razin (1960) suppression (seen for 11 of the 14 events from 12192). The Razin effect, or ionized-medium emissivity suppression (R. Ramaty 1969; D. A. Guidice & J. P. Castelli 1975), is the attenuation of radiation in a medium when the index of refraction is less than one. Such suppression requires high density in the flaring loops. Although A. L. Lysenko et al. (2023) did not do a direct check against LASCO coronagraph data, they proposed that the majority of the cold solar flares they considered were confined flares.

4.2.2. *Potential Applications of the Microwave Spectrum Indicator of Confinement/Eruption for Strong Solar and Stellar Flares*

Even with complete coronagraph coverage today, outages occur—some produced by the Sun itself, e.g., during solar particle-induced "snowstorms" in coronagraph images such as occurred during the "Halloween" episode of strong activity in 2003 October–November (N. Gopalswamy et al. 2005a, 2005b). The 410 MHz signature of CME generation indicates that two M-class flares from NOAA AR 10486 that occurred early on October 29 during a snowstorm were eruptive.

This study was prompted in part by an analysis of eruptive and confined flares in spot group 5395 in March 1989 (work in progress). While this period did have Solar Maximum Mission coronagraph coverage, the lower sensitivity, larger occulting disk, and longer image cadence of this instrument resulted in a correction factor of ~2, meaning that half of all CMEs would be missed (D. F. Webb & R. A. Howard 1994). Microwave spectra could be used to distinguish between confined and eruptive events for times after the establishment of a robust radio patrol of the Sun in the mid-1960s (H. Tanaka et al. 1973) and before routine coronagraph coverage began with the launch of SOHO LASCO in late 1995.

A third application for a microwave spectrum discriminator between confined and eruptive flares is the search for CMEs (or their absence) in association with stellar flares (A. F. Kowalski 2024). Stellar CMEs are much more difficult to observe than stellar flares. The marked mismatch between the numbers of observations of the two phenomena led to the suggestion that CMEs could be suppressed by the large spot groups and inferred strong overlying fields of active flare stars (J. J. Drake et al. 2016; S.-P. Moschou et al. 2019). More recently, A. M. Veronig et al. (2021, 2025) showed that observation of stellar coronal dimmings in EUV and X-ray emission is a promising technique for comprehensive detection of CMEs on stars. The large spot group area of NOAA AR 12192 (E. W. Cliver et al. 2022b) and its effect on microwave spectra demonstrated here suggests that observing active flare stars at 410 MHz for evidence of CME confinement during flares (absence of emission at 410 MHz) or CME occurrence (presence of such emission) is an additional technique that can be used to distinguish between eruption and confinement in stellar flares. The Very Large Array observing band from 224 to 480 MHz should be well suited for such monitoring of solar-type stars.

Acknowledgments

M.L. acknowledges the Space It Up project funded by the Italian Space Agency, ASI, and the Ministry of University and Research, MUR, under contract No. 2024-5-E.0 - CUP No. I53D24000060005. S.W. thanks AFOSR for support for basic research through LRIR 23RVCOR003. The views expressed herein are those of the authors and do not reflect official guidance of the US Government or Dept of Defense.

ORCID iDs

E. W. Cliver https://orcid.org/0000-0002-4342-6728
M. Kazachenko https://orcid.org/0000-0001-8975-7605
H. S. Hudson https://orcid.org/0000-0001-5685-1283
T. Alberti https://orcid.org/0000-0001-6096-0220
M. Laurenza https://orcid.org/0000-0001-5481-4534
S. M. White https://orcid.org/0000-0002-8574-8629
P. T. Gallagher https://orcid.org/0000-0001-9745-0400

References

Akasofu, S.-I., & Yoshida, S. 1967, P&SS, 15, 39
Alberti, T., & Cliver, E. W. 2025, Harvard Dataverse, V1, doi:10.7910/DVN/MNJ9AV
Avallone, E. A., & Sun, X. 2020, ApJ, 893, 123
Bougeret, J. L., Goetz, K., Kaiser, M. L., et al. 2008, SSRv, 136, 487
Bougeret, J.-L., Kaiser, M. L., Kellogg, P. J., et al. 1995, SSRv, 71, 231
Brueckner, G. E., Howard, R. A., Koomen, M. J., et al. 1995, SoPh, 162, 357
Cai, Z. M., Zhang, Q. M., Ning, Z. J., Ji, H. S., et al. 2021, SoPh, 296, 61
Cane, H. V. 2000, SSRv, 93, 55
Canfield, R. C., Reardon, K. P., Leka, K. D., et al. 1996, ApJ, 464, 1016
Chen, H., Zhang, J., Ma, S., et al. 2015, ApJL, 808, L24
Cheng, X., Zhang, J., Ding, M. D., Guo, Y., & Su, J. T. 2011, ApJ, 732, 87
Cliver, E. W., & D'Huys, E. 2018, ApJ, 864, 48
Cliver, E. W., Mekhaldi, F., & Muscheler, R. 2020, ApJL, 900, L11
Cliver, E. W., Nitta, N. V., Thompson, B. J., & Zhang, J. 2004, SoPh, 225, 105
Cliver, E. W., Pötzi, W., & Veronig, A. M. 2022a, ApJ, 938, 136
Cliver, E. W., Schrijver, C. J., Shibata, K., & Usoskin, I. G. 2022b, LRSP, 19, 2
Cliver, E. W., Webb, D. F., & Howard, R. A. 1999, SoPh, 187, 89
Cliver, E. W., White, S. M., & Balasubramaniam, K. S. 2011, ApJ, 743, 145
Crooker, N. U., Gosling, J. T., & Kahler, S. W. 2002, JGR, 107, 1028
Dennis, B. R., & Zarro, D. M. 1993, SoPh, 146, 177
Desai, M., & Giacalone, J. 2016, LRSP, 13, 3
Drake, J. J., Cohen, O., Garraffo, C., & Kashyap, V. 2016, in IAU Symp. 320, Solar and Stellar Flares and their Effects on Planets, ed. A. G. Kosovichev, S. L. Hawley, & P. Heinzel (Cambridge: Cambridge Univ. Press), 196
Dungey, J. W. 1961, PhRvL, 6, 47
Fairfield, D. H., & Cahill, L. J., Jr. 1966, JGR, 71, 155
Gopalswamy, N. 2006, JApA, 27, 243
Gopalswamy, N., Barbieri, L., Cliver, E. W., et al. 2005a, JGR, 110, A09S00
Gopalswamy, N., Michałek, G., Yashiro, S., et al. 2024, arXiv:2407.04165
Gopalswamy, N., Yashiro, S., Liu, Y., et al. 2005b, JGR, 110, A09S15
Gopalswamy, N., Yashiro, S., Michalek, G., et al. 2009, EM&P, 104, 295
Gopalswamy, N., Yashiro, S., Xie, H., et al. 2008, ApJ, 674, 560
Gosling, J. T. 1993, JGR, 98, 18937
Gosling, J. T., Hildner, E., MacQueen, R. M., et al. 1976, SoPh, 48, 389
Gosling, J. T., McComas, D. J., Phillips, J. L., & Bame, S. J. 1991, JGR, 96, 7831

Guidice, D. A., & Castelli, J. P. 1975, SoPh, 44, 155
Guidice, D. A., Cliver, E. W., Barron, W. R., & Kahler, S. 1981, BAAS, 13, 553
Harrison, R. A. 1995, A&A, 304, 585
Hudson, H. S. 1991, BAAS, 23, 1064
Hudson, H., Cliver, E., White, S., et al. 2024b, SoPh, 299, 39
Hudson, H. S., Acton, L. W., Alexander, D., et al. 1995, in AIP Conf. Proc. 382, Solar Wind Eight, ed. D. Winterhalter et al. (Melville, NY: AIP), 88
Hudson, H. S., & Cliver, E. W. 2001, JGR, 106, 25199
Hudson, H. S., Cliver, E. W., Fletcher, L., et al. 2024a, MNRAS, 532, 3120
Kahler, S. 1977, ApJ, 214, 891
Kahler, S. W., Hildner, E., & Van Hollebeke, M. A. I. 1978, SoPh, 57, 429
Kahler, S. W., Reames, D. V., & Sheeley, N. R., Jr. 2001, ApJ, 562, 558
Kahler, S. W. 1992, ARA&A, 30, 113
Kahler, S. W., & Ling, A. G. 2022, ApJ, 934, 175
Kaiser, M. L., Kucera, T. A., Davila, J. M., et al. 2008, SSRv, 136, 5
Kay, H. R. M., Culhane, J. L., Harra, L. K., & Matthews, S. A. 2003, AdSpR, 32, 1051
Kazachenko, M. D., Albelo-Corchado, M. F., Tamburri, C., & Welsch, B. T. 2022a, SoPh, 297, 5
Kazachenko, M. D., Lynch, B. J., Savcheva, A., Sun, X., & Welsch, B. T. 2022b, ApJ, 926, 56
Kazachenko, M. D., Lynch, B. J., Welsch, B. T., & Sun, X. 2017, ApJ, 845, 49
Kazachenko, M. D. 2023, ApJ, 958, 104
Klein, K. L., Trottet, G., & Klassen, A. 2010, SoPh, 263, 185
Kondo, T., Isobe, T., Iji, S., Watari, S., & Tokumaru, M. 1995, J. Commun. Res. Lab., 42, 111
Kopp, R. A., & Pneuman, G. W. 1976, SoPh, 50, 85
Kowalski, A. F. 2024, LRSP, 21, 1
Kurokawa, H. 1989, SSRv, 51, 49
Laurenza, M., Cliver, E. W., Hewitt, J., et al. 2009, SpWea, 7, S04008
Leblanc, Y., Dulk, G. A., & Bougeret, J.-L. 1998, SoPh, 183, 165
Lemen, J. R., Title, A. M., Akin, D. J., et al. 2012, SoPh, 275, 17
Li, T., Chen, A., Hou, Y., et al. 2021, ApJL, 917, L29
Li, T., Hou, Y., Yang, S., et al. 2020, ApJ, 900, 128
Lysenko, A. L., White, S. M., Zhdanov, D. A., et al. 2023, ApJ, 954, 122
Machol, J., Viereck, R., Peck, C., & Mothersbaugh, J., III 2022, GOES XRS Operational Data (NOAA), Technical Report, University of Colorado
McCracken, K. G. 1962, JGR, 67, 447
Moore, R. L., Sterling, A. C., Hudson, H. S., & Lemen, J. R. 2001, ApJ, 552, 833
Moschou, S.-P., Drake, J. J., Cohen, O., et al. 2019, ApJ, 877, 105
Nakajima, H., Sekiguchi, H., Sawa, M., et al. 1985, PASJ, 37, 163
Namekata, K., Ichimoto, K., Ishii, T. T., & Shibata, K. 2022, ApJ, 933, 209
Neupert, W. M. 1968, ApJ, 153, L59
Newton, H. W. 1943, MNRAS, 103, 244
Pallavicini, R., Serio, S., & Vaiana, G. S. 1977, ApJ, 216, 108
Ramaty, R. 1969, ApJ, 158, 753
Razin, V. A. 1960, IzVUZ, 3, 584
Rust, D. M. 1983, SSRv, 34, 21
Sheeley, N. R., Jr., Bohlin, J. D., Brueckner, G. E., et al. 1975, SoPh, 45, 377
Sheeley, N. R., Jr., Howard, R. A., Koomen, M. J., & Michels, D. J. 1983, ApJ, 272, 349
Shibata, K., & Magara, T. 2011, LRSP, 8, 6
Shimojo, M., & Iwai, K. 2023, GSDJ, 10, 114
Shimojo, M., & Shibata, K. 2000, ApJ, 542, 1100
Sui, L., Holman, G. D., & Dennis, B. R. 2006, ApJL, 645, L157
Sun, X., Bobra, M. G., Hoeksema, J. T., et al. 2015, ApJL, 804, L28
Švestka, Z. 2007, SoPh, 246, 393
Švestka, Z., & Cliver, E. W. 1992, in Proc. IAU Coll. 133, Eruptive Solar Flares, ed. Z. Svestka, B. V. Jackson, & M. E. Machado (New York: Springer), 1
Tan, C.-M., Klein, K. L., Yan, Y.-H., et al. 2021, RAA, 21, 274
Tanaka, H., Castelli, J. P., Covington, A. E., et al. 1973, SoPh, 29, 243
Temmer, M. 2021, LRSP, 18, 4
Thalmann, J. K., Su, Y., Temmer, M., & Veronig, A. M. 2015, ApJL, 801, L23
Tschernitz, J., Veronig, A. M., Thalmann, J. K., Hinterreiter, J., & Pötzi, W. 2018, ApJ, 853, 41
Veronig, A., Temmer, M., Hanslmeier, A., Otruba, W., & Messerotti, M. 2002, A&A, 382, 1070
Veronig, A. M., Dissauer, K., Kliem, B., et al. 2025, LRSP, 22, 138
Veronig, A. M., Muhr, N., Kienreich, I. W., Temmer, M., & Vršnak, B. 2010, ApJL, 716, L57
Veronig, A. M., & Polanec, W. 2015, SoPh, 290, 2923
Veronig, A. M., Odert, P., Leitzinger, M., et al. 2021, NatAs, 5, 697
Vourlidas, A., Balmaceda, L. A., Xie, H., & St. Cyr, O. C. 2020, ApJ, 900, 161
Wang, Y., & Zhang, J. 2007, ApJ, 665, 1428
Webb, D. F., & Howard, R. A. 1994, JGR, 99, 4201
White, S. M., Shimojo, M., Iwai, K., et al. 2024, ApJ, 969, 3
Yashiro, S., Akiyama, S., Gopalswamy, N., & Howard, R. A. 2006, ApJL, 650, L143
Zhang, J., Dere, K. P., Howard, R. A., Kundu, M. R., & White, S. M. 2001, ApJ, 559, 452